LARGE EDDY SIMULATION OF COMPRESSIBLE JETS LADEN WITH GROWING ICE PARTICLES

Ephi Maglaras and François Garnier
Atmospheric Environment Unit
Physics Department
ONERA
BP 72
92322 Châtillon, France
Ephi.Maglaras@onera.fr
Francois.Garnier@onera.fr

ABSTRACT

In order to understand the process of formation of condensation trail (contrail), the flow in the near field of an engine jet is studied by using the Large Eddy Simulation technique. The configuration consists of a hot round jet laden with soot particles. The particles are tracked by the Lagrangian approach and their growth is calculated by a microphysics model of water vapour condensation and ice formation. A series of simulations has been performed with a low Mach number ($M = 0.2$) and a moderate one ($M = 1$) at realistic Reynolds number ($Re = 3.2 \cdot 10^6$). Whatever the Mach number used the ice crystals first appear at the edges of the jet where the hot and moist flow mixes with the cold and dry ambient air. The simulations show that the growth process is controlled both by the thermal transfers and the mass coupling which are more important for the low Mach number case.

INTRODUCTION

The condensation trails, or contrails, which often form behind the aircraft, may have an impact on cloudiness and may affect the Earth's radiative budget balance (Académie des Sciences, and Académie Nationale de l'Air et de l'Espace, 1997). The engine jet emits hot and moist air which is progressively diluted with the cold and dry atmosphere. When the partial pressure of water vapour reaches the saturation vapour pressure, the mixing becomes supersaturated over liquid (ice), and then the water vapour condenses and freezes to form a visible contrail in the sky. This phenomenon is favoured by the turbulence of the jet flow and by the condensation sites emitted by the engine (mainly soots coming from the incomplete combustion). Nevertheless, the understanding of these processes is still limited and needs further studies.

This work is based on 3-dimensionnal Large Eddy Simulations (LES) of a turbulent hot jet laden with soot particles, which represents a complex issue involving multi-scale phenomena such as jet turbulence and microphysics. We will study more specifically the compressibility effects on the particle evolution by comparing two numerical simulations: one with a low Mach number 0.2 to simulate a quasi-incompressible flow and the other with a Mach number equal to 1 to be close to real flight conditions. After the description of the modelling used for the gas-phase composed of the mixing air-vapour and for the solid phase constituted of soot particles and ice crystals, we will discuss the results.

MODELLING

We consider the temporal evolution of a turbulent hot jet composed of the miscible species air and water vapour, laden with solid (soot) particles. The dynamics of the two phases are distinct (Eulerian and Lagrangian approaches), whereas the gas and the dispersed phase are supposed to be in thermal balance. In this work, the gas-phase is governed by the compressible Navier-Stokes equations together with a transport equation for the water vapour and the solid phase by a Lagrangian equation together with a growth model.

Gas-phase equations

The LES approach for a compressible flow consists in applying a spatial filter on the compressible Navier-Stokes equations so that any dimensionless variable $\phi(x) = \left[\rho_g, \rho_g u_i, E_g, \rho_g Y_v\right]$, where ρ_g is the density of the gas constituted of the mixing air-vapour, u_i its velocity, E_g its total energy, and Y_v represents the vapour mass ratio. Each variable is decomposed into a resolved part $\overline{\phi(x)}$ and a non-resolved (or subgrid-scale) part $\phi''(x)$ with $\phi(x) = \overline{\phi(x)} + \phi''(x)$. For compressible flows, we use the

Favre filter (1965) defined as $\tilde{\phi} = \overline{\rho_g \phi} / \overline{\rho}_g$. With this approach, the dimensionless Navier-Stokes equations become:

$$\frac{\partial \overline{\rho}_g}{\partial t} + \frac{\partial}{\partial x_i}\left(\overline{\rho}_g \tilde{u}_i\right) = 0 \tag{1}$$

$$\frac{\partial}{\partial t}\left(\overline{\rho}_g \tilde{u}_i\right) + \frac{\partial}{\partial x_j}\left(\overline{\rho}_g \tilde{u}_i \tilde{u}_j\right) + \frac{\partial \overline{p}_g}{\partial x_i} - \frac{1}{Re}\frac{\partial \tilde{\sigma}_{ij}}{\partial x_j} = -\frac{\partial \tau_{ij}}{\partial x_j} \tag{2}$$

$$\frac{\partial \overline{E}_g}{\partial t} + \frac{\partial\left[\left(\overline{E}_g + \overline{p}_g\right)\tilde{u}_i\right]}{\partial x_i} - \frac{1}{Re}\frac{\partial\left(\tilde{\sigma}_{ij}\tilde{u}_i\right)}{\partial x_i} - \frac{\partial}{\partial x_i}\left(\frac{\mu_g\left(\tilde{T}_g\right)}{Re\,Pr(\gamma-1)M^2}\frac{\partial \tilde{T}_g}{\partial x_i}\right) =$$

$$\frac{\partial Q_i}{\partial x_i} - \frac{\partial \tau_{ij}\tilde{u}_i}{\partial x_i} + \tau_{ij}\frac{\partial \tilde{u}_i}{\partial x_i} + \frac{1}{Re}\Theta \tag{3}$$

$$\frac{\partial}{\partial t}\left(\overline{\rho}_g \tilde{Y}_v\right) + \frac{\partial}{\partial x_i}\left(\overline{\rho}_g \tilde{Y}_v \tilde{u}_i\right) - \frac{1}{Re\,Pr}\frac{\partial}{\partial x_i}\left(\mu_g\left(\tilde{T}_g\right)\frac{\partial \tilde{Y}_v}{\partial x_i}\right) + \overline{\omega} = -\frac{\partial \xi_i}{\partial x_i} \tag{4}$$

The source term $\overline{\omega}$ is the rate of condensed matter and is calculated using heterogeneous nucleation theory, so it is a mass coupling term which will be defined in the next section. Note that the coupling terms which should appear in Eq. (1) to (3) are assumed to be negligible, mainly due to the low mass ratio between the solid (ice) phase and the gaseous mixing (air and water).

The subgrid-scale (SGS) stress tensor $\tau_{ij} = \overline{\rho}_g\left(\widetilde{u_i u_j} - \tilde{u}_i \tilde{u}_j\right)$, the SGS heat flux $Q_i = \frac{1}{\gamma - 1}\left(\overline{p_g u_i} - \overline{p}_g \tilde{u}_i\right)$ and the SGS vapour flux $\xi_i = \overline{\rho}_g\left(\widetilde{Y_v u_i} - \tilde{Y}_v \tilde{u}_i\right)$ are modelled by the Smagorinsky model hybridized by the Liu-Meneveau-Katz one, defined below.

$$\tau_{ij} = \frac{1}{2}\left[-\overline{\rho}_g \underbrace{(C_s\Delta)^2\left|S(\tilde{\mathbf{u}})\right|}_{\mu_{sm}} S_{ij}(\tilde{\mathbf{u}}) + \widehat{\left(\overline{\rho}_g \tilde{u}_i \tilde{u}_j\right)} - \frac{\widehat{\overline{\rho}_g \tilde{u}_i}\,\widehat{\overline{\rho}_g \tilde{u}_j}}{\hat{\overline{\rho}}_g}\right] \tag{5}$$

with

$$\left|S(\tilde{\mathbf{u}})\right|^2 = \frac{1}{2} S_{ij}(\tilde{\mathbf{u}}) S_{ij}(\tilde{\mathbf{u}}) \tag{6}$$

$$Q_i = \frac{1}{2}\left[-\frac{\overline{\rho}_g \mu_{sm}}{(\gamma-1)Pr_t M^2}\frac{\partial \tilde{T}_g}{\partial x_i} + \frac{1}{(\gamma-1)\gamma M^2}\left(\widehat{\overline{\rho}_g \tilde{T}_g \tilde{u}_i} - \frac{\widehat{\overline{\rho}_g \tilde{T}_g}\,\widehat{\overline{\rho}_g \tilde{u}_i}}{\hat{\overline{\rho}}_g}\right)\right] \tag{7}$$

$$\xi_i = \frac{1}{2}\left[-\overline{\rho}_g \mu_{sm}\frac{\partial \tilde{Y}_v}{\partial x_i} + \frac{\partial}{\partial x_i}\left(\widehat{\overline{\rho}_g \tilde{Y}_v \tilde{u}_i} - \frac{\widehat{\overline{\rho}_g \tilde{Y}_v}\,\widehat{\overline{\rho}_g \tilde{u}_i}}{\hat{\overline{\rho}}_g}\right)\right] \tag{8}$$

where the Smagorinsky constant is $C_s = 0.2$, Δ is the cut-off length scale associated to the filter $(\bar{\cdot})$ and $\hat{\Delta} = \Delta\sqrt{6}$ the one associated to the filter $(\hat{\cdot})$. The turbulent Prandtl number is set to 0.7. The SGS dissipation term $\Theta = \overline{\sigma_{ij}\frac{\partial u_j}{\partial x_i}} - \overline{\sigma}_{ij}\frac{\partial \tilde{u}_j}{\partial x_i}$ is modelled as Ghosal et al. (1995) did:

$$\Theta = C_\varepsilon \overline{\rho}_g \frac{k^{3/2}}{\Delta} \tag{9}$$

with the SGS kinetic energy $k = \frac{\mu_{sm}^{\ 2}}{\Delta^2}$ and the dynamic coefficient defined by Vreman (1995) as $C_\varepsilon = \frac{\int_\Omega\left[(1-\gamma)\frac{\partial Q_i}{\partial x_i} + \frac{\partial}{\partial x_i}\left(\tau_{ij}\tilde{u}_j\right) - \tau_{ij}\frac{\partial \tilde{u}_j}{\partial x_i}\right]d\Omega}{\int_\Omega \overline{\rho}_g \frac{k^{3/2}}{\Delta} d\Omega}$.

In their work on jet flows, Ferreira Gago et al. (2003) have shown that this modelling leads to best results.

Solid-phase equations

In the Lagrangian approach, each particle is followed individually. They are considered to be spherical with the radius r_p. They are supposed to be passive due to their small size, i.e. they have the same velocity as the carrier phase. For the LES, we use the filtered flow velocity, which amounts to neglecting direct SGS effects on particle evolution, as done by Leboissetier et al. (2005). On neglecting the gravity forces because of their small size, their movement is then governed by the equation:

$$\frac{d\mathbf{x}_p}{dt} = \tilde{\mathbf{u}} \tag{10}$$

The growth of the ice particle is calculated by solving the equation of Fukuta-Walter microphysical theory (1970) given by:

$$r_p \frac{dr_p}{dt} = \frac{S - A}{C_T A + C_\rho} \tag{11}$$

where S is the saturation ratio (ratio between the partial vapour pressure P_v and the saturation vapour pressure P_{sat}), A describes the Kelvin effect and is the ratio of the vapour pressure at the water droplet surface (before freezing) to the saturated vapour pressure over a flat surface at the droplet temperature, (C_T) and (C_ρ) represent factors associated with the surface of growing and evaporating particle. These factors inevitably control the water vapour density and the temperature of air just above the surface. All these terms are

calculated with the filtered fluid thermodynamical parameters evaluated at the particle location. Thus we obtain the mass variation of each ice crystal and a fortiori the vapour mass variation which leads to the coupling term in Eq. (4). As the numerical density of soots is high (about 10^{12} according to the IPCC (2000)) we use a further modelling to minimize the simulation cost, which consists in carrying on computational particles, each one representing n physical particles. Finally, $\bar{\omega}$ is given by the relation:

$$\bar{\omega}(x) = \frac{\bar{r}^3}{Y_{v0}} \cdot \frac{1}{V(x)} n \sum_{k=1}^{n_p} \rho_p 4\pi r_p^2 \frac{dr_p}{dt} \qquad (12)$$

where Y_{v0} is the reference vapour mass ratio, $\bar{r}$ is the ratio between the reference soot radius and the reference domain length, and n_p is the number of particles with the density ρ_p contained in the filtering volume $V(x)$.

Numerical methods and initial configuration

The fluid equations are solved by a sixth order compact scheme in space (Lele, 1992) and by a third order Runge-Kutta algorithm for time integration. We add a MSOU Superbee limiter for the scalar equation (4). The gas flow and particle equations are coupled at each time step of the computation. The position of the particle is calculated from Eq. (10) using a fourth-order Adams-Bashforth method. Finally, the particle radius is computed by solving Eq. (11) with a fourth-order Runge-Kutta scheme.

The computational domain is rectangular and the grid is uniform in all directions with $\Delta x = \Delta y = \Delta z = 0.1 r_j$ with $r_j = 0.5\text{m}$ the jet radius. The cross plane extends from $x, z = -11 r_j$ to $11 r_j$ and the streamwise extent of the computational box is $L_y = 12 r_j$. All the fluid reference variables are the core jet values. The length of the axial direction is chosen according to the results obtained by the stability analysis of Michalke and Herman (1982). The jet axial velocity is initialized by using a *tanh* profile. Note that a similar expression is used for the initial scalar (vapour) profile while the temperature is initialized according to the Crocco-Buseman law (Panda et al., 2001). A non-reflexive boundary condition is used for the cross flow domain and periodic condition is employed in the axial direction.

Whatever the simulation performed ($M = 1$ or $M = 0.2$) the jet Reynolds number is fixed to $Re = 3.2 \cdot 10^6$, the jet temperature is $T_j = 440\text{K}$, twice the ambient one, the vapour molar ratio in the jet core is $X_{v0} = 0.03$ whereas the ambient air is totally dry. We initially load $5 \cdot 10^{10}$ soot particles in the jet (with $n = 10^6$) with the same radius $r_0 = 20\text{nm}$ (monodispersed distribution). Such conditions have been used by Paoli et al. (2004).

A schematic of the flow configuration is presented in Figure 1.

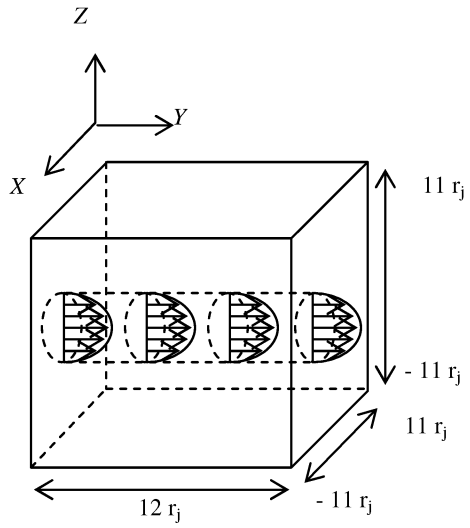

Figure 1. Schematic of the initial flow configuration

RESULTS

Two simulations have been performed during 2.5 seconds, knowing that the characteristic time of the $M = 1$ simulation is five times higher than in the low Mach number simulation. We first display in Figure 2 the distribution of ice crystal size at the end of the simulation in terms of PDF radius (Probability Density Function).

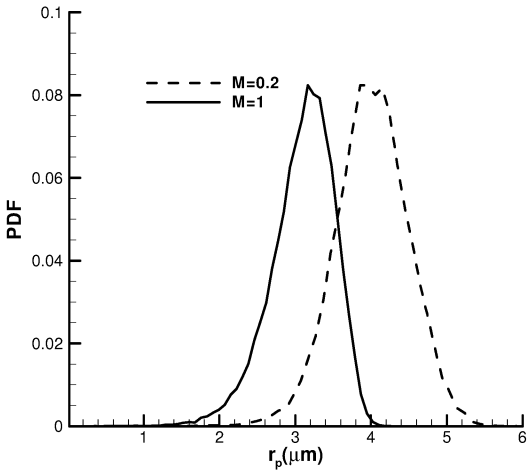

Figure 2. Distribution of particle radii

In the case of $M = 0.2$, the particle mean size reached 4μm versus 3μm for the compressible case (i.e. $M = 1$). We also notice that the shape of the PDF finally approaches a Gaussian profile which indicates polydispersion of ice crystal radii. Furthermore the mean saturation ratio is plotted as a function of time in Figure 3.

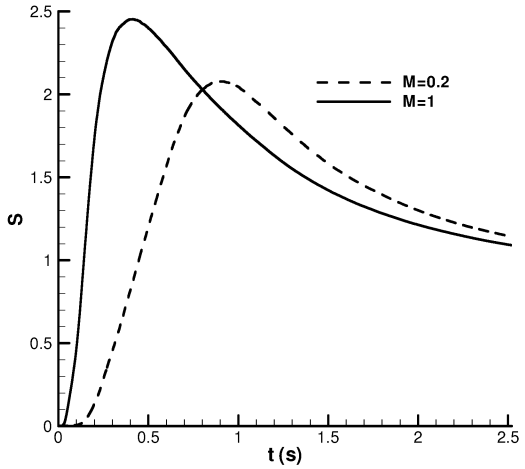

Figure 3. Temporal evolution of the mean saturation ratio

When half particles are supersaturated, i.e. at $t = 0.15$ s for $M = 1$ and $t = 0.49$ s for $M = 0.2$, the mean saturation ratio S is equal to 1. This ratio reaches a maximum value at $t = 0.41$ s for $M = 1$ and $t = 0.90$ s for $M = 0.2$ and is higher in the case where the Mach number is higher.

Moreover, on plotting cross planes of the jet in the two cases when the particles start to saturate (Figure 4), we notice that the ice crystals first appear at the edges of the jet, where the hot and moist flow mixes with the cold and dry ambient air.

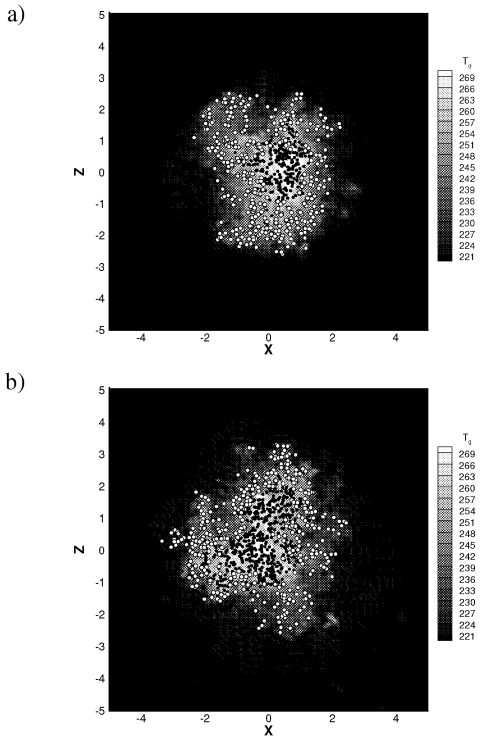

Figure 4. Y-plane cut with contours of gas temperature T_g (grey scale), dry soots (black points) and ice crystals (white points). a) $M = 0.2$ at $t = 0.49$s. b) $M = 1$ at $t = 0.15$s.

In this figure where the temperature contours are displayed, we also see that at this time the jet has cooled considerably, going from 440K to 270K.

Figure 5 compares the temporal evolution of the particle mean mass with respect to the two Mach numbers considered.

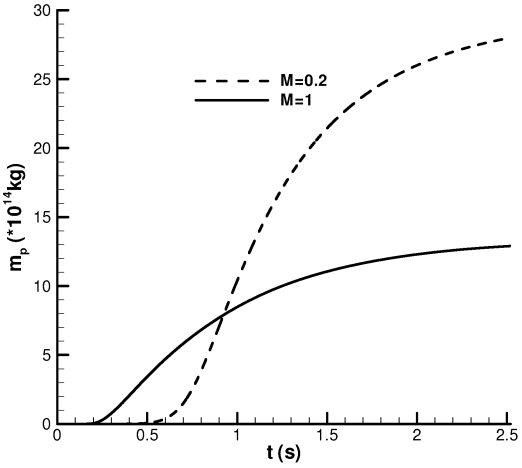

Figure 5. Temporal evolution of particle mean mass

The figure quantitatively shows that the growth of the particle mass starts earlier for $M = 1$. The mean mass increases very rapidly, with a maximum growth rate dm_p/dt at $t = 0.41$s for $M = 1$ and $t = 0.90$s for $M = 0.2$, as reported in Figure 6. Nevertheless, this rate which is much lower for $M = 1$ (more than twice) than this calculated for $M = 0.2$. After that the growth slows down, as the saturation ratio S (Figure 3) and the rate of growth (Figure 6) decrease.

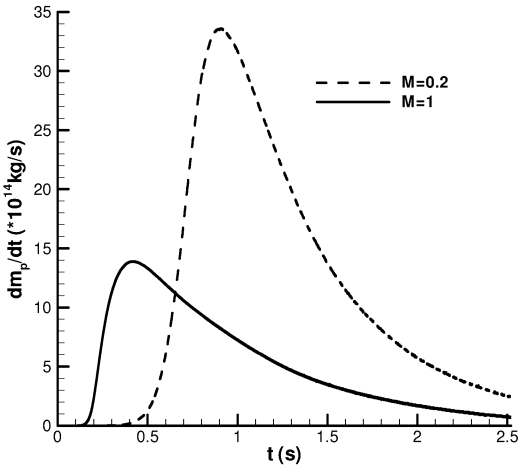

Figure 6. Mean rate of particle growth

Now it is a matter of understanding why the particle radii are smaller in the compressible flow. For this we have to look at the thermodynamical parameters which are used in the Fukuta-Walter model. All these physical parameters are obtained as a function of temperature (latent heat, thermal diffusion and conduction) and vapour partial pressure P_v, or the vapour volume ratio (used for the saturation ratio). So we interpolate the temperature and the vapour mass ratio of the fluid at the point where each particle is located. We plot in Figure 7 the mean vapour partial pressure P_v and the saturation vapour pressure P_{sat} as functions of the mean temperature T around particles.

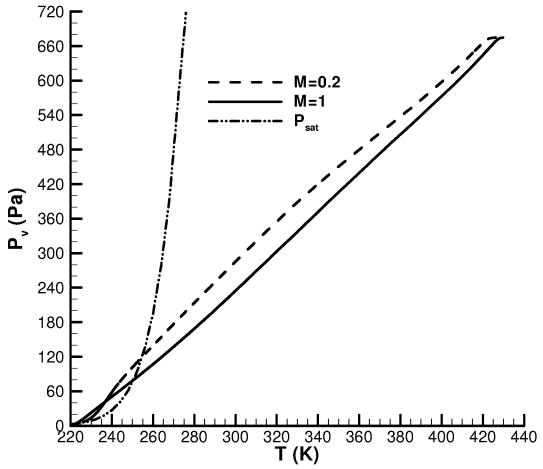

Figure 7. Vapour partial pressure as function of temperature

When the saturation conditions have been reached, i.e. when $P_v(T)$ crosses the saturation curve $P_{sat}(T)$ (and a fortiori when $S=1$) the vapour is less diluted for the $M=0.2$ computation ($P_v=119\text{Pa}$) than in the compressible case ($P_v=79\text{Pa}$). In fact, at the beginning of the $M=0.2$ computation, the temperature decreases faster than the vapour is diluted, whereas for $M=1$, the evolution of $P_v(T)$ is quasi -linear. This explained by observing strong heat diffusion fluxes for the $M=0.2$ case (see the term $1/M^2$ in Eq. (3)). Indeed, the profiles of the mean temperature at the same dimensionless times (Figure 8) (where $t_0=\dfrac{r_j}{M\cdot c(T_j)}$ with $c(T_j)$ the speed of sound at the jet temperature T_j) exhibit a more important decrease for the case $M=0.2$.

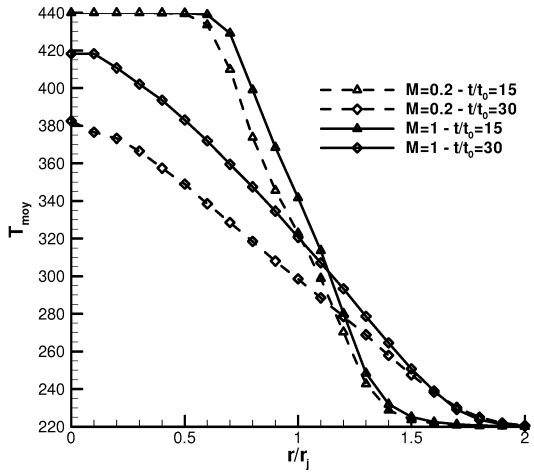

Figure 8. Profiles of mean temperature

We now observe what happens after the condensation has begun. Turning now to a zoom view of the saturation curve as reported in Figure 9.

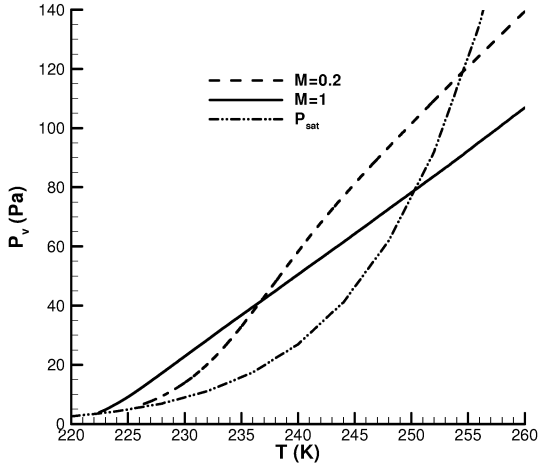

Figure 9. $P_v(T)$ after the saturation

For $M=0.2$, the curve $P_v(T)$ changes its behaviour after the start of the condensation: the water vapour disappears more rapidly than the temperature decreases, whereas $P_v(T)$ still exhibits a similar linear evolution. To understand this behaviour of the vapour molar ratio, which is calculated in Eq. (4), we examine the only term of this equation which is likely to be different in the two simulations, i.e. the coupling term $\bar{\omega}$. We display in Figure 10 the temporal evolution of this term as it appears in Eq. (4), considering the mean value of the particle growth. We notice that this term is very high for $M=0.2$ ($\bar{\omega}=8.5\cdot10^{-4}$ at $t=0.90\text{s}$ while the mean vapour molar ratio around particles is $X_v=2\cdot10^{-3}$) and there is a factor of nearly 10 with the other case (for which $\bar{\omega}=7\cdot10^{-5}$ at $t=0.41\text{s}$ when $X_v=1\cdot10^{-3}$). This term is obviously

maximum when dm_p/dt and S are maximum (cf. Figures 3 and 6).

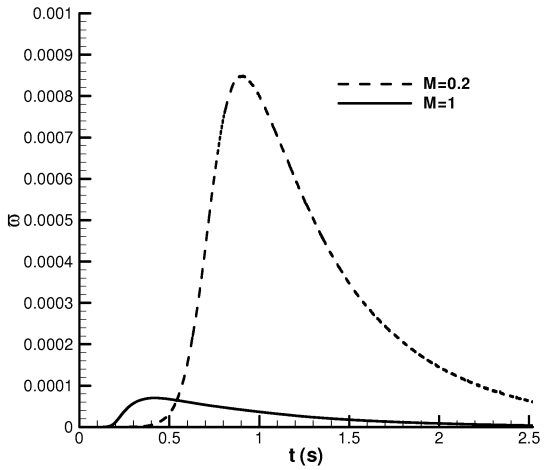

Figure 10. Temporal evolution of the coupling term $\bar{\omega}$

As a result the coupling between the fluid/solid phases is more important in the case $M = 0.2$ as compared with the case $M = 1$, since $P_v(T)$ evolves linearly during the simulation. It is due to the evolution of the vapour molar ratio: when the condensation starts, the vapour is more diluted for $M = 1$, which we can see in the Figure 11 where the vapour contours are more developed than in the case $M = 0.2$.

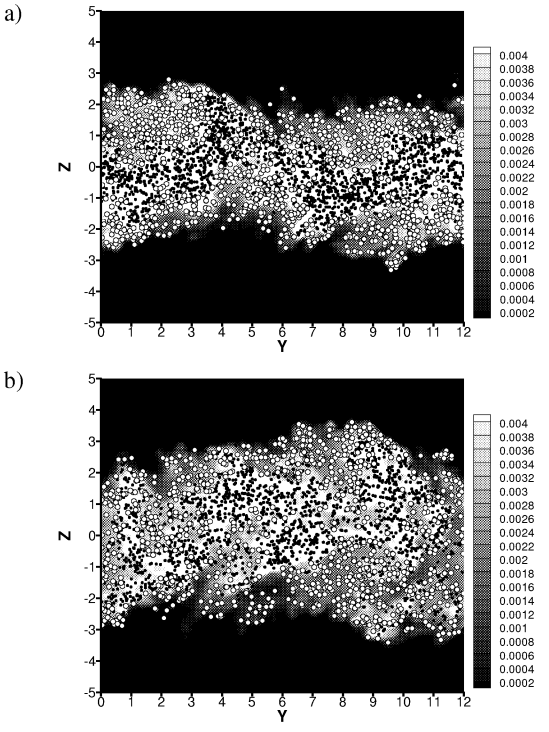

Figure 11. X = 0 plane cut with contours of X_v (grey scale), dry black soots and white ice crystals. a) $M = 0.2$ at $t = 0.49s$. b) $M = 1$ at $t = 0.15s$.

CONCLUSION

In this study, we have conducted Large Eddy Simulation of a turbulent jet flow laden with soot particles. In one case we had quasi-incompressible conditions ($M = 0.2$) and in the other we have initialised the flow with $M = 1$ to be close to real flight conditions. The results show that the growth of the ice crystals is more important for the $M = 0.2$ case. The maximum rate of growth is nearly twice higher than in the compressible case since the vapour is less diluted when the mixing reaches the saturation conditions. It is due to the strong thermal transfers occurring at the beginning of the $M = 0.2$ computation. Moreover, the coupling term between the gas/solid phases has not a similar influence: its effect is more important at $M = 0.2$. Nevertheless, in spite of an initial monodispersed distribution, the particle radius distribution finally approaches a Gaussian profile which indicates polydispersion of ice crystal radii.

REFERENCES

Académie des Sciences, and Académie Nationale de l'Air et de l'Espace, 1997, "Impact de la flotte aérienne sur l'environnement atmosphérique et le climat", *Institut de France*, Rapport n°40.

Favre, A., 1965, "Equations des gaz turbulents compressibles", *Journal de Mécanique*, Vol. 4, pp. 361-390.

Ferreira Gago, C., Garnier, F., and Utheza, F., 2003, "Direct testing of subgrid scale models in large-eddy simulation of a non-isothermal turbulent jet", *International Journal for Numerical Methods in Fluids*, Vol. 42, pp. 999-1026.

Fukuta, N., and Walter, L. A., 1970, "Kinetics of Hydrometeor Growth from a Vaper-Spherical Model", *Journal of Atmospheric Sciences*, Vol. 27, No. 8, pp. 1160-1172.

Ghosal, S., Lund, T. S., Moin, P., and Akselvoll, K., 1995, "A Dynamic Localization Model for Large-Eddy Simulation of Turbulent Flows", *Journal of Fluid Mechanics*, Vol. 286, pp. 229-255.

Leboissetier, A., Okong'o, N., and Bellan, J., 2005, "Consistent large-eddy simulation of a temporal mixing layer laden with evaporating drops. Part 2. *A posteriori* modelling.", *Journal of Fluid Mechanics*, Vol. 523, pp. 37-78.

Lele, S. K., 1992, "Compact Finite Difference Schemes with Spectral-Like Resolution", *Journal of Computational Physics*, Vol. 103, pp. 16-42.

Michalke, A., and Herman, G., 1982, "On the inviscid instability of a circular jet with external flow", *Journal of Fluid mechanics*, Vol. 114, pp. 343-359.

Panda, J., Zaman, K. B. M. Q., and Seasholtz, R. G., 2001, "Measurements of Initial Conditions at Nozzle Exit of High Speed Jets", *AIAA Paper*, 2001-2143.

Paoli, R., Hélie, J., and Poinsot, T., 2004, "Contrail formation in aircraft wakes", *Journal of Fluid Mechanics*, Vol. 502, pp. 361-373.

Vreman, B., 1995, "Direct and Large-Eddy Simulation of the compressible turbulent mixing layer", *Thesis of the University of Twente.*